The Effect of Anisotropic Dispersion on the Convective Mixing in Long-Term CO_2 Storage in Saline Aquifers

Karim Ghesmat, Hassan Hassanzadeh, and Jalal Abedi
Dept. of Chemical and Petroleum Engineering, University of Calgary, Calgary, AB T2N 1N4, Canada

DOI 10.1002/aic.12292
Published online May 26, 2010 in Wiley Online Library (wileyonlinelibrary.com).

Carbon dioxide storage in deep saline aquifers is considered a possible option to bring greenhouse gas emissions under control. The understanding of the underlying mechanisms, such as convective mixing and associated mechanisms, affecting this mixing may have an impact on the long-term sequestration process in deep saline aquifers. One of the significant aspects of the flow of miscible species in porous media is velocity dependent dispersion. The effect of dispersion on dissolution of carbon dioxide (CO_2) into brine is investigated by full nonlinear numerical simulations. This study reveals that dispersion may dramatically change the trend of CO_2 dissolution into brine. It was found that the dissolution of CO_2 increases as dispersion strength increases. The mixing pattern also shows three different mechanisms: diffusion, convection, and a highly nonlinear interaction mechanism. However, the medium dispersivity ratios were found to slightly affect the mixing, while having an impact on the fingering pattern. © 2010 American Institute of Chemical Engineers *AIChE J,* 57: 561–570, 2011
Keywords: transport, porous media, mixing

Introduction

The main greenhouse gas from the combustion of fossil fuel is carbon dioxide (CO_2), one of the major contributors to climate change while different studies on the capture and sequestering of CO_2 are currently being performed; geological sequestration is an immediate option and a technologically feasible process. Carbon dioxide may be sequestrated in various geological formations, such as depleted oil and gas reservoirs, uneconomical coal beds for coal bed methane recovery, and deep saline aquifers. One of the many geologic CO_2 sequestration options is the injection into saline aquifers that are capable of storing large volumes of CO_2 from power plants without the need for long transport pipelines.

The major concern of CO_2 storage is the potential for CO_2 leakage through imperfect confinement. Upon injection of CO_2 into saline aquifers, CO_2 may be stored by various trapping mechanisms. In fact, several mechanisms are involved in the storage process. Some gas may be trapped as residual gas saturation (residual gas trapping),[1] or by dissolution into the brine,[2–4] and some gas may react with host minerals to precipitate carbonates[5–7] (mineral trapping).

In this work, our focus is only on solubility trapping, where CO_2 is trapped by dissolution in brine. Once CO_2 is injected into a saline aquifer, it dissolves into the formation brine and saturates the fresh brine as it migrates upward due to its buoyancy. Brine with dissolved CO_2 will be denser than resident formation brine; and, due to gravity override, the boundary layer is unstable. This instability results in a convective mixing, which, in turn, increases CO_2 dissolution into brine. Different properties, such as adverse mobility ratio, medium heterogeneity, and anisotropic dispersion, may have significant impacts on such diffusive boundary layer instability.

One of the aspects that may be important in the sequestration of CO_2 is dispersion phenomena. Dispersion usually

Correspondence concerning this article should be addressed to J. Abedi at jabedi@ucalgary.ca.

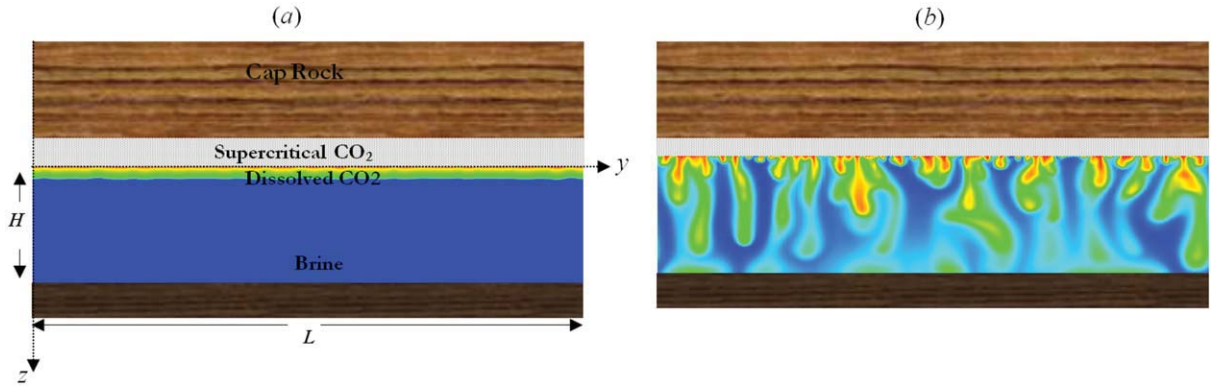

Figure 1. A schematic of the CO_2 sequestration process: (a) early in the process and (b) late in the process.

[Color figure can be viewed in the online issue, which is available at wileyonlinelibrary.com.]

affects the solute transport in porous media. Since the early 1950s, there has been active interest in this topic, motivated mainly by applications in oil recovery and contaminant elimination from underground. Depending on the media characteristics and also on the fluid properties, dispersion of the solute in the media is expected to be influenced. This may be, in part, due to the fact that there is no definite dispersion model for variable viscosity and/or density driven displacements in porous media. Still, there have been a few attempts to analyze the role of dispersion by incorporating various models that were developed for capillary flow or were based on continuum models. Some of these studies have focused on the linear stability analysis of the flow.

In particular, in a pioneering work, Tan and Homsy[8] performed a linear stability for a system with an anisotropic dispersion coefficient, where the authors considered a linear relationship between the velocity field and the dispersion coefficients in the flow and transverse directions, while crossflow coefficients were set to be zero. Their results indicated that the small transverse dispersion led to an increase in the growth rate and a shift to smaller fingers, while large transverse dispersion totally stabilized the displacement.

A subsequent analysis using a transversely isotropic dispersion tensor with a fixed ratio of transverse to longitudinal dispersivity was conducted by Yortsos and Zeybek.[9] The stability analysis focused on the flow with a velocity-dependent dispersion coefficient. Following convection-dispersion formalism, the base state at conditions of unfavorable mobility contrast was analyzed. It was found that the velocity dependence of the dispersion induced a destabilizing influence at short wavelengths. This effect, which was in contrast to the stabilizing effects commonly associated with dispersion, was highly pronounced near the onset of the displacement. Zimmerman and Homsy[10,11] conducted a full nonlinear simulation for a system with adverse viscosity ratio and anisotropic dispersion. Other works, such as miscible quarter five-spot displacements,[12] stability analysis of miscible flows in a radial Hele-Shaw cell[13] and effect of dispersion on viscous fingering,[14] can be considered as works related to anisotropic dispersion for different flow systems in porous media.

Dispersion can be considered a very important factor in an aquifer that may highly affect the solute migration. As shown by Gelhar et al.,[15] the reservoirs and aquifers may have a wide range of dispersivity coefficients, depending on the type of medium. The authors conducted a critical review of dispersivity observation from 59 different field sites. The information was developed by compiling extensive tabulations of information on aquifer type, hydraulic properties, flow configuration, type of monitoring network, tracer, method of data interpretation, overall scale of observation and longitudinal, horizontal transverse, and vertical transverse dispersivities from original sources. They found that the data indicated a trend of systematic increase of the longitudinal dispersivity with an observation scale, but the trend was much less clear when the reliability of the data was considered. The longitudinal dispersivities ranged from 10^{-2} to 10^{-5} m, and the ratio of transverse to longitudinal dispersivity coefficient was shown to vary from 0.1 to 1. The early studies by Bear suggested that the dispersion tensor is velocity-dependent, while more complex approaches based on stochastic, continuum and network models have also been used to analyze dispersion in real porous media and explained such dependency.[16,17]

In what follows, we aim to incorporate the dispersion model presented by Bear and Bachmat[18] to find out how anisotropic dispersion may influence the CO_2 sequestration process. A full nonlinear simulation is presented following a quantitative analysis of the flow system.

Mathematical Model

In the current study, we consider a vertical rectilinear geometry, in which dissolved CO_2 with its larger density is on top of the brine, which is less dense. The supercritical CO_2 ($scCO_2$) usually accumulates at the top of aquifer and is dissolved into the brine.

Figure 1a depicts the geometry considered here, where the dissolved CO_2 is denser than the resident formation brine and likely makes the interface between CO_2 and the resident brine unstable, resulting in convective mixing. The supercritical phase is assumed to be thermodynamically in equilibrium with the brine, such that the constant concentration of dissolved CO_2 can be established at the CO_2-brine interface. Figure 1b shows the behavior of the system late in the process, during the convective mixing. In the present study, only the miscible unstable front was studied and examined numerically.

To elucidate how anisotropic dispersion may influence the convective mixing during the CO_2 sequestration process, a set of partial differential equations governing the above flow system is required to be solved numerically. The governing equations are the equation of motion (Darcy's equation), the convection-diffusion equation and the equation of continuity. The Boussinesq approximation is assumed here to simplify the continuity equation, where the density variation due to CO_2 dissolution is considered to be very small. Accordingly, we may treat density, ρ, as a constant in all terms in the equations of motion, except the one in the external force. This assumption has been validated in some studies.[19] The equations are:

$$\mathbf{u} = -\frac{K}{\mu}\left(\nabla P - \rho g\,\widehat{\mathbf{e}}\right) \tag{1}$$

$$\phi\frac{\partial c}{\partial t} + \mathbf{u}.\nabla c = \phi(\nabla.\mathbf{D}.\nabla c) \tag{2}$$

$$\nabla.\mathbf{u} = 0 \tag{3}$$

$$\rho = \rho_0 + \Delta\rho c_a \tag{4}$$

where C and ρ represent concentrations of the dissolved CO_2 and fluid density, respectively, while K, μ, $\mathbf{u}$, P, and ϕ represent medium permeability, fluid viscosity, the Darcy velocity vector, pressure and medium porosity, respectively. The density is also assumed to vary with the concentration of dissolved CO_2, such that $\Delta\rho$ represents the density difference between CO_2 saturated brine and the resident formation brine. It is necessary to mention that, in our analysis, the porous medium is isotropic and only the dispersion is anisotropic. In fact, for an isotropic medium, the fourth rank dispersion tensor is related to only two constants.[18] The dispersion tensor, $\mathbf{D}$, is considered velocity dependent. In general form, the dispersion tensor along the flow streamline is expressed as[18]:

$$\mathbf{D} = D_0\mathbf{I} + \mathbf{D}_m = \begin{bmatrix} D_0 & 0 \\ 0 & D_0 \end{bmatrix} + \begin{bmatrix} a_{\mathrm{L}}|\mathbf{u}| & 0 \\ 0 & a_{\mathrm{T}}|\mathbf{u}| \end{bmatrix} \tag{5}$$

where D_0 and $\mathbf{D}_m$ are the molecular diffusion coefficient and the mechanical dispersion contribution, respectively, and $\mathbf{I}$ represents the identity matrix. Here, a_{L} and a_{T} are referred to as the dispersivity coefficients and can be considered to represent the strength of the dispersion in the longitudinal and transverse directions, respectively. We perform an orthogonal transformation to formulate the dispersion tensor in the fixed Cartesian reference frame. The new dispersion tensor is:

$$\mathbf{D} = (D_0 + a_{\mathrm{T}}|\mathbf{u}|)\mathbf{I} + (a_{\mathrm{L}} - a_{\mathrm{T}})\frac{\mathbf{u}\mathbf{u}^{\perp}}{|\mathbf{u}|} \tag{6}$$

The mechanical dispersion tensor in the transformed space can be shown as:

$$\mathbf{D}_m = \frac{1}{u^2+v^2}\begin{bmatrix} u^2a_L|\mathbf{u}| + v^2a_{\mathrm{T}}|\mathbf{u}| & uva_L|\mathbf{u}| - uva_{\mathrm{T}}|\mathbf{u}| \\ uva_L|\mathbf{u}| - uva_{\mathrm{T}}|\mathbf{u}| & v^2a_L|\mathbf{u}| + u^2a_{\mathrm{T}}|\mathbf{u}| \end{bmatrix} \tag{7}$$

One should note that the dispersion tensor is generally anisotropic, except when $a_{\mathrm{L}} = a_{\mathrm{T}}$ or in the absence of flow. It is also worth mentioning that, when $a_{\mathrm{L}} = a_{\mathrm{T}}$, the dispersion tensor is isotropic, but not constant and varies linearly with the norm of the velocity vector. The boundary conditions, which are required for a CO_2 sequestration process are:

$$c(y,0,t) = c_0 \quad \frac{\partial c(y,H,t)}{\partial z} = 0 \tag{8}$$

$$c(0,z,t) = c(L,z,t) \quad c(0,z,t) = c(L,z,t) \quad v(0,z,t) = v(L,z,t) \tag{9}$$

$$u(y,0,t) = v(y,0,t) = 0 \quad u(y,H,t) = v(y,H,t) = 0 \tag{10}$$

The aspect ratio of the geometry is defined as $A = L/H$. We need to mention that the boundary conditions in the y-direction are considered to be periodic. The problem is solved only for one slice of the aquifer. The required initial conditions are:

$$c(y,z,0) = c_0 \qquad u(y,z,0) = v(y,z,0) = 0 \tag{11}$$

For convenience, the above set of equations are made dimensionless as $u^* = u,v/u_b$, $c^* = c/c_0$, $t^* = tu_b/\phi H$, $P^* = P/\Delta\rho gH$, and z^*, $y^* = z$, y/H, where u_{b} is the maximum buoyancy velocity defined as $u_b = K\Delta\rho g/\mu$. Equations 1–4 are reformulated into the new form and, after dropping the superscripts, we obtain:

$$\mathbf{u} = -(\nabla P - \rho\hat{\mathbf{e}}) \tag{12}$$

$$\frac{\partial c}{\partial t} + \mathbf{u}.\nabla c = \frac{1}{Ra}(\nabla.\mathbf{D}.\nabla c) \tag{13}$$

$$\nabla.\mathbf{u} = 0 \tag{14}$$

$$\rho = \rho_0 + c_a \tag{15}$$

By substituting the dispersion tensor in the convection-diffusion equation, we end up with the following equation:

$$\begin{aligned} &\frac{\partial c}{\partial t} + u\frac{\partial c}{\partial z} + v\frac{\partial c}{\partial y} \\ &= \frac{1}{Ra}\,\frac{\partial}{\partial z}\left[\frac{\partial c}{\partial z} + \left(S(\alpha|\mathbf{u}|-1) + S(1-\alpha)\frac{u^2}{|\mathbf{u}|}\right)\frac{\partial c}{\partial z}\right. \\ &\quad \left. + \left(S(1-\alpha)\frac{uv}{|\mathbf{u}|}\right)\frac{\partial c}{\partial y}\right] + \frac{\partial}{\partial y}\left[\frac{\partial c}{\partial y} + \left(S(1-\alpha)\frac{uv}{|\mathbf{u}|}\right)\frac{\partial c}{\partial z}\right. \\ &\quad \left. + \left(S(\alpha|\mathbf{u}|-1) + S(1-\alpha)\frac{v^2}{|\mathbf{u}|}\right)\frac{\partial c}{\partial y}\right] \end{aligned} \tag{16}$$

where S and α are two-dimensional numbers that represent the longitudinal dispersion strength and dispersivity ratio, respectively, as given by:

$$\alpha = \frac{a_{\mathrm{T}}}{a_{\mathrm{L}}} \qquad S = \frac{a_{\mathrm{L}}u_{\mathrm{b}}}{D_0 + a_{\mathrm{L}}u_{\mathrm{b}}} \tag{17}$$

Accordingly, a larger S represents a system with stronger longitudinal dispersion, and a smaller α describes a flow system that is strongly anisotropic.

It can be clearly seen that both α and S cannot be larger than one. We take the curl of Darcy's equation to eliminate the pressure term from equations, resulting in:

$$\frac{\partial v}{\partial z} - \frac{\partial u}{\partial y} = -\frac{\partial \rho}{\partial y} \tag{18}$$

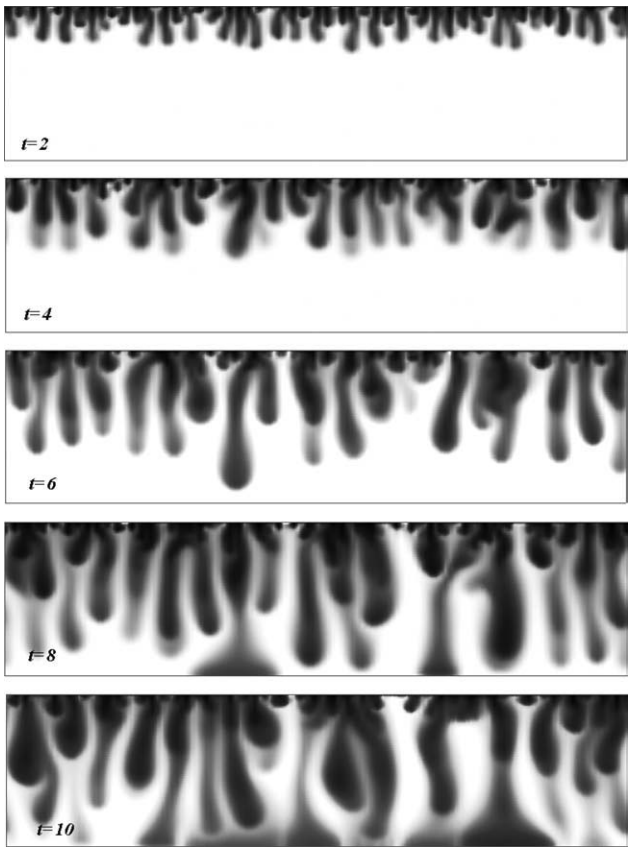

Figure 2. Time trace concentration contours of dissolved CO_2 in brine for $S = 0.5$, $\alpha = 0.5$, and $Ra = 1000$.

Ra represents the Rayleigh number and $Ra = K\Delta\rho gH/\phi D_L\mu$, where D_L is $D_L = D_0 + a_L u_b$. The boundary and initial conditions are also changed in the new formulation:

$$c(y,0,t) = 1 \qquad \frac{\partial c(y,l,t)}{\partial z} = 0 \tag{19}$$

$$c(0,z,t) = c(A,z,t) \quad u(0,z,t) = u(A,z,t) \quad v(0,z,t) = v(A,z,t) \tag{20}$$

$$u(y,0,t) = v(y,0,t) = 0 \qquad u(y,1,t) = v(y,1,t) = 0 \tag{21}$$

$$c(y,z,0) = 1 \qquad u(y,z,0) = v(y,z,0) = 0 \tag{22}$$

The Rayleigh number range of analyses is between 500 and 1000, based on the data provided for the different aquifers.[3] The authors have shown that the Rayleigh numbers for the aquifers subject to convection are in the range 200–1000.

To numerically solve the equations, the equations are reformulated into vorticity and stream function formulations. The velocity field can be written as:

$$u = \frac{\partial \psi}{\partial y}, \qquad v = -\frac{\partial \psi}{\partial z} \tag{23}$$

The reformulated equations are:

$$\nabla^2 \psi = -\omega \tag{24}$$

$$\frac{\partial c}{\partial t} = -\frac{\partial \psi}{\partial y}\frac{\partial c}{\partial z} + \frac{\partial \psi}{\partial z}\frac{\partial c}{\partial y} + (\nabla.\mathbf{D}.\nabla c) \tag{25}$$

$$\omega = -\frac{\partial c}{\partial y} \tag{26}$$

The same boundary and initial conditions as Eqs. 19–22 are applied here.

Numerical Approach

The dynamic complexity of dispersive flows in porous media and around the boundary layer requires the use of highly accurate numerical methods to investigate the problem. The nonlinearity in both the momentum and convection-diffusion equations and the sharp changes in density profile at the gas-liquid interface are well known to lead to a stiff numerical problem that requires high performing and numerically stable algorithms. To solve the problem, a second-order finite difference is implemented in the z-direction, while a highly accurate spectral method is used in the transverse direction. Perturbations are introduced at the boundary and a semi-implicit time discretization is also used to conduct a full numerical simulation. Typically, 250×256 nodes are used in the simulation for high values of Rayleigh number. Since the scheme is not fully implicit in time, simulations occasionally show numerical instability at high values of Rayleigh numbers ($Ra > 1000$), as well as for small values of the ratio of the dispersivity coefficients ($\alpha < 0.1$). To overcome the problem, correction-evaluation and under-relaxation schemes were iterated until the desired convergence criterion, which had been set to 10^{-4}, was accomplished. The numerical convergence was checked with a comparison of the results for different mesh numbers. The code has been also validated for different geometries in a previous study.[14]

Results and Discussion

We attempted to perform a systematic examination for different scenarios to realize how the dispersion strength (S) and medium dispersivity ratio (α) may affect the instability for an unstable diffusive boundary layer during a CO_2 sequestration process. The domain aspect ratio is selected in such a way that the length of the domain is much larger than the wavelength of the instabilities. The simulations started by introducing small disturbances in the concentration field around the boundary layer indicated in Figure 1a. We initially represented how the instability may develop for moderate dispersive and anisotropic flow system. We also initially considered the fingering mechanisms and the development for an anisotropic dispersive system, following a discussion on impact of the dispersion strength and medium dispersivity on the dissolution of CO_2 into brine. A two-dimensional nonlinear stability analysis was carried out here with the expectation that the results for averaged quantities will not be different when the third dimension is included. A recent study for nondispersive CO_2 sequestration has revealed that the results for two- and three-dimensional analyses are close to each other with a negligible difference.[20] However, it has been previously shown[21] that, when the fluid is injected at an angle to the direction of gravity, the two- and three-dimensional fingering results are different.

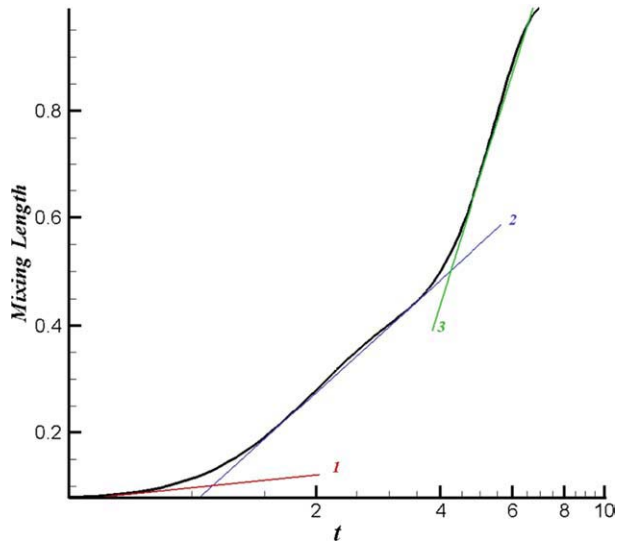

Figure 3. Mixing length variation with time for $S = 0.5$, $\alpha = 0.5$, and $Ra = 1000$.

[Color figure can be viewed in the online issue, which is available at wileyonlinelibrary.com.]

Instability development

Figure 2 illustrates time trace concentration contours for $S = 0.5$, $\alpha = 0.5$, and Ra is equal to 1000. The concentration maps indicate the time evolution of instabilities. The fingering pattern seems strong and nonlinear interactions can be found at large times. Different mechanisms, such as merging or splitting, may also be realized at longer times. In fact, the perturbations that are introduced at early time grow gradually resulting long fingers at late time interacting nonlinearly.

To determine how the concentration of dissolved CO_2 is affected by the hydrodynamics of the flow system or may vary during the sequestration process, the mixing length is plotted and shown in Figure 3. The mixing length is defined as the length measured from the boundary to the place where the average transverse concentration is larger than or equal to 0.01. This length can reveal the trend of instability growth over time. In fact, the increment of the mixing length represents the growth of fingers, such that a larger mixing length is an indication of larger fingers and, in turn, larger growth of instability.

Three different zones can be clearly distinguished from the mixing length variation. These zones are shown by three different numbers on Figure 3 (1, 2, and 3). The length initially (zone 1) changes with a smaller slope than the other zones. As the measured slope in the first zone indicates that mixing length changes with $t^{0.5}$, one can conclude that the diffusion mechanism is initially dominant. This can be attributed to the diffusion stage, where the convective forces are not significant enough to affect the hydrodynamics of the flow system. A transition then occurs; and, the mixing length enters into the second stage, where the variation is faster and the perturbations have grown (zone 2). The time during which the transition begins may be attributed to the onset of convection. The vector analysis can clearly reveal that the velocity vectors are relatively larger than earlier in the process, such that convection can play a major role in the mass transportation. This can be simply observed from Figure 2 where, between time traces 2 and 4, fingers have developed, representing the existence of convective mixing.

Another transition occurs, and the mixing length changes are quicker (zone 3). This zone corresponds to strong convection, where nonlinear interaction can be clearly realized from the concentration contours. Indeed, the perturbations are enough large at longer times to result in larger velocity vectors in both directions. These large velocities, in turn, result in the interaction of the fingers, faster growth of the fingers, and faster growth of the mixing zone and length. The current analysis was tested for $Ra = 500$ and 1000, and all of the cases clearly indicate these three zones of transition. These zones can be considered as a general trend in which the mixing area varies linearly in each zone.

Further analysis can be conducted by the calculation of the concentration/longitudinal-velocity covariance, which is a measure of how concentration and longitudinal velocity change together. The covariance is calculated as:

$$\mathrm{Cov}(c,u) = E[(c - E(c)).(u - E(u))] \tag{27}$$

Figure 4 illustrates the trend of covariance variation with time, where the covariance initially increases as time passes, reaching a maximum, but decreases over a longer period time. In fact, this reveals that the variation of the longitudinal velocity to concentration is initially slower, representing diffusion dominance; however, it varies faster at later in the process, when convection becomes important. This may be attributed to the fast growth of perturbations in the early stage when convection starts. The peak represents the time that the fingers reach the bottom of the aquifer and the medium becomes saturated by dissolved CO_2. Indeed, the fingers expand more laterally when touching the bottom of aquifer and result in a weakening of the longitudinal velocity. In the decreasing stage, the variation of the dissolved CO_2 concentration and velocity magnitude is slower, as the medium is more occupied by the dissolved CO_2 and finds a more homogenous profile. At very late times in the process, when

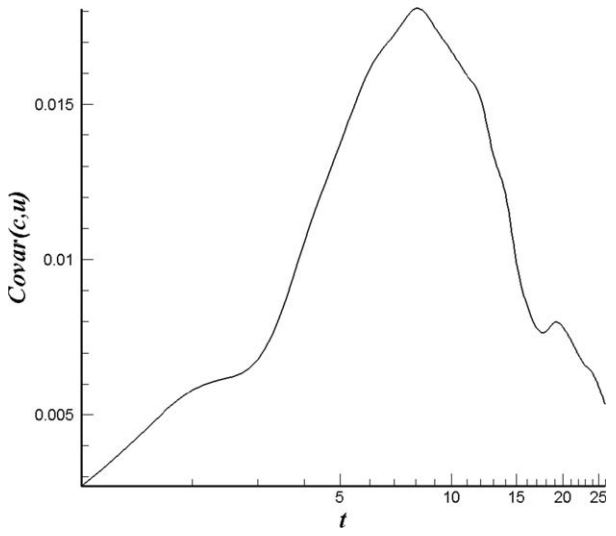

Figure 4. Concentration/longitudinal-velocity covariance variation with time for $S = 0.5$, $\alpha = 0.5$, and $Ra = 1000$.

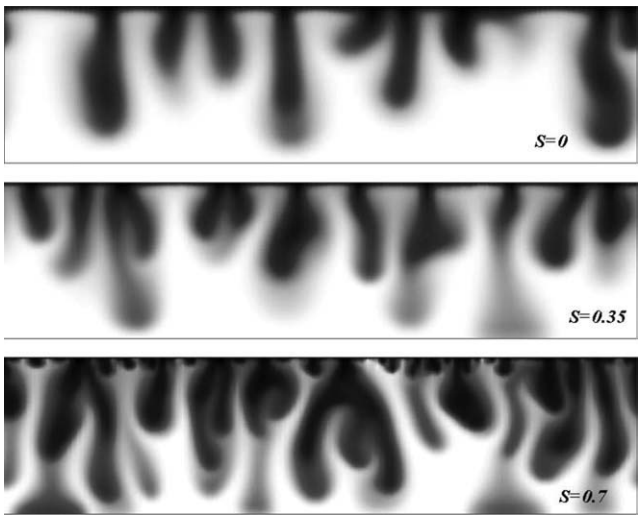

Figure 5. Effect of dispersion strength on the instability development at $t = 9$, $Ra = 500$, and $\alpha = 0.2$.

the aquifer is highly saturated by dissolved CO_2, the variation of the concentration/velocity is less pronounced and the rate of covariance changes becomes smaller.

Effect of dispersion strength on the instability

A previous study dealing with the effects of dispersion on a horizontal miscible flow system, where one fluid was injected into the porous medium, showed that the medium dispersivity term had an important effect on the instability growth.[14] Further investigation was performed in this study to find out how dispersion may affect the flow system and, specifically, the dissolution of CO_2 in brine. It is necessary to mention that, when S is equal to zero, this corresponds to an isotropic system with only a molecular diffusion coefficient, while a large S corresponds to the highly dispersive flow system. In this study, we consider three different dispersion strengths: $S = 0$ (isotropic system, no dispersion), $S = 0.35$ (moderate dispersive system) and $S = 0.7$ (highly dispersive system).

Figure 5 depicts the change in the instability development as the dispersion strength increases. It can be observed that the fingering pattern dramatically changes as the dispersion is enhanced, such that more fingers and highly nonlinear interactions can be found as the dispersion strength increases. The trend of instability is totally different for a small dispersion strength than that for a large one. The fingers also touch the bottom of the aquifer faster when the flow system is highly dispersive, representing more dissolution of CO_2 into the brine. In fact, one may notice that a larger dispersion strength means a smaller ratio of either viscous forces or diffusion to the buoyancy forces in the longitudinal direction. Accordingly, larger buoyancy forces, in turn, result in faster growth of perturbations over time, which can cause a more complicated structure of fingers and also more dissolution of CO_2 into brine. Indeed, this should result in larger velocity vectors and higher convective mixing.

As velocity plays a relatively large role on the dispersive flow systems, a snapshot of velocity vectors has been plotted, which are overshadowed on the concentration contours in Figure 6. The absolute velocity values for different cases discussed in Figure 5 indicate larger values as the dispersion strength increases. The velocity vectors in Figure 6 represent a strong interfinger flow. The circulation of flow can be also found around the finger tips, where brine and dissolved CO_2 are circulated and mixing occurs. The velocity magnitude gets smaller far from the fingers. As mentioned, the velocity vector magnitude increases as the dispersion strength increases for the same Rayleigh number. Consequently, one may expect stronger mixing when the flow system is dispersive. More examination may be conducted using quantitative analysis of different parameters. We measured the average amount of dissolved CO_2 into brine, the mixing length as previously described, and the area swept by the dissolved CO_2.

We performed a quantitative analysis to show the effect of dispersion to a greater extent. Figure 7 depicts the average mixing length for different dispersion strengths. The curves clearly show the three different regions discussed in Figure 3, where diffusion is initially dominant and convective mixing is the dominant mechanism involved in the mixing process. It can be seen that the mixing length is initially larger when the dispersion strength is small, but the trend changes later and becomes larger for more dispersive systems. As shown, the velocities reach higher values for dispersive flows, resulting in a faster growth of fingers. Accordingly, one may expect that mixing length grows faster for dispersive cases at later times, when the convection is dominant.

As the dispersion is velocity dependent (Eq. 6), we may categorize the mass transfer mechanisms into diffusion and convection-dispersion. Since the system is initially at a stationary condition, diffusion is the dominant process. However, the concentration gradient in the transverse direction (y-direction) is stronger early in the process, which can result

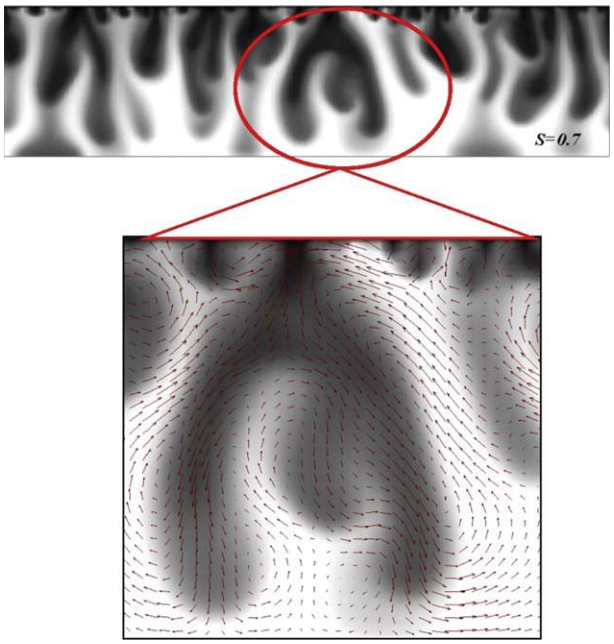

Figure 6. A snapshot of velocity vectors for a highly dispersive system $S = 0.7$, $\alpha = 0.2$, and $Ra = 500$.

[Color figure can be viewed in the online issue, which is available at wileyonlinelibrary.com.]

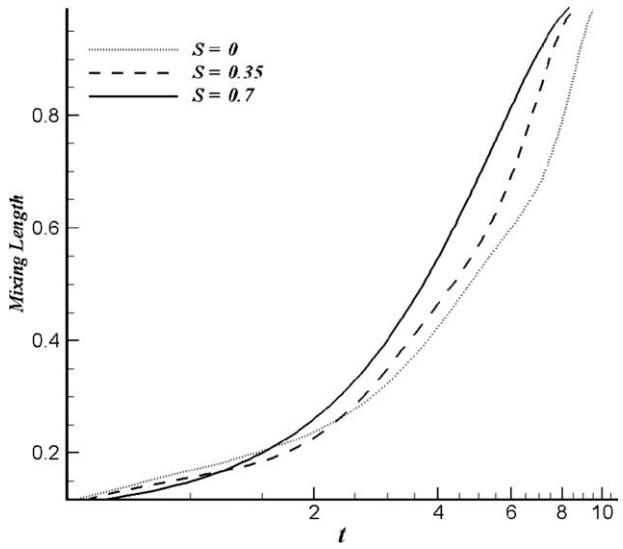

Figure 7. Mixing length variation for different dispersion strength values at $\alpha = 0.2$ and $Ra = 500$.

in vortices and, in turn, a stronger velocity field. To investigate this, we needed to examine the hydrodynamics of the flow system early in the process. Figure 8 illustrates the overshadowing of the velocity vectors on the concentration field for two limiting scenarios, $S = 0$ and $S = 0.7$, in an early phase. The picture clearly shows that the velocity vectors are much larger in the dispersive case than in the nondispersive one. Indeed, the length of the vectors represents their magnitude.

It can be observed that the boundary layer remains diffusive for nondispersive flows, while perturbations have grown considerably for dispersive systems. For a dispersive flow system, the circulation around the finger tips brings the CO_2 undersaturated brine upwards and mixes with the CO_2 saturated brine. However, the mass transfer is dominated by an isotropic diffusion ($\alpha = 1$) in all directions for nondispersive systems early in the process, resulting in a more diffusive boundary layer and, in turn, a longer mixing length. The mass transfer mechanism becomes totally convection; and, dispersion dominates later in the process, as the velocity magnitude gets large enough. In general, one can conclude that diffusion plays a more significant role in the early phase for nondispersive flow systems than for dispersive ones. This may be the reason that mixing lengths may initially develop faster in nondispersive systems.

Using mixing length variation, one may notice that the onset of convection is faster for dispersive systems. This can be simply realized using the change in the slope of the mixing length curve, similar to what is shown in Figure 3, representing a transition from the diffusion stage to the convective stage, as indicated in Figure 7. To further advance the above discussion, we conducted an additional investigation by measuring the average concentration of dissolved CO_2 in brine for the whole domain and also by the mass flux at the boundary. Figure 9 indicates the variation of the average dissolved concentration of CO_2 into brine. It can be revealed that the curves follow a trend similar to the mixing length, such that it is initially higher for nondispersive system, but becomes smaller later for the nondispersive case. The three zones of transitions can be also distinguished here.

Although the differences are small for moderate dispersive and nondispersive systems, the highly dispersive flow system shows a gap from the two other cases. Consequently, this may represent a high rate of mass transfer of CO_2 at the boundary. The mass flux can be measured at the boundary, by taking an average of the concentration gradient along the boundary. Figure 10 illustrates the variation of the CO_2 mass flux at the boundary. The curves show fluctuations in the later stage of the process, which may be attributed to a large value for the velocity magnitude in all directions, which, in turn, results in a high nonlinear interaction of the fingers. Again, we find a higher flux early in the process for a nondispersive system, when diffusion is dominant; whereas there is a higher rate of flux for dispersive systems in the later stage, when convection becomes the dominant mechanism.

The mass flux at the top boundary initially decreases, as diffusion controls the mechanism of mass transportation and makes the concentration profile relatively even. The first peak may represent the onset of convection, when the flux increases very rapidly. As shown before, this may take longer for a system with no dispersion or with moderate dispersion strength. The convection enhances mixing, and this is the reason that the flux increases at the boundary; however, the flux then decreases continuously. As times goes by, the medium becomes saturated with dissolved CO_2, and the total average of concentration increases. Accordingly, this may result in a reduction in flux at the boundary.

Effect of medium dispersivity on the instability

The collected data by Gelhar et al.[15] shows that the medium dispersivity ratio may change in a wide range between 0.1 and 1, depending on the type of reservoir or aquifer. We

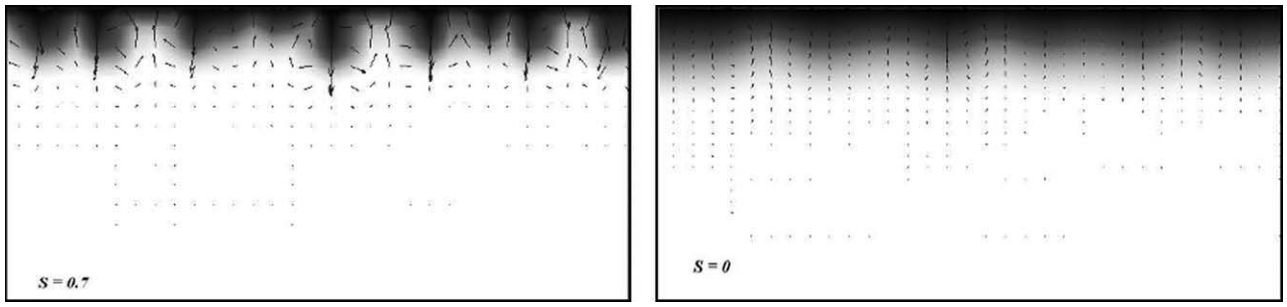

Figure 8. Snapshot of velocity vectors for two different S, $Ra = 500$ early in the process ($t = 1$).

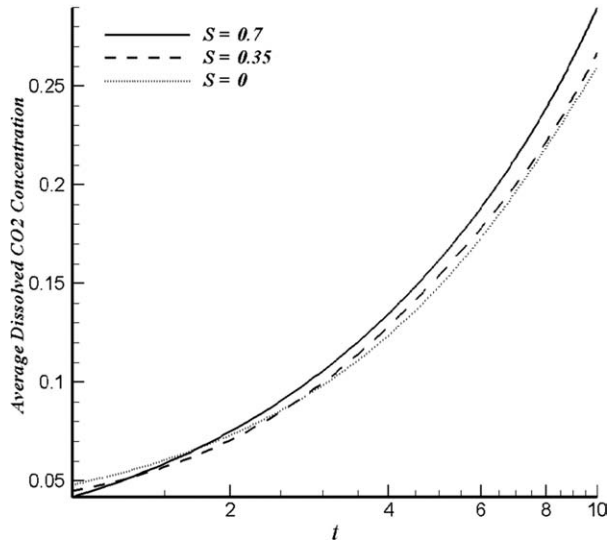

Figure 9. Variation of average concentration of dissolved carbon dioxide in brine over time for different dispersion strength values at $\alpha = 0.2$ and $Ra = 500$.

considered four different scenarios in which the flow system was highly dispersive, but the medium dispersivity ratios varied from 0.1 to 1. Figure 11 illustrates the instability development for a highly dispersive system ($S = 0.7$) at different medium dispersivity ratios. The fingering pattern indicates different mechanisms, including merging and splitting, for different cases. The concentration maps also reveal that medium dispersivity affects the instability development late in the process.

Our analysis shows that the impact of medium dispersivity ratios early in the process is not considerable, but they influence the patterns as time passes, when the velocity magnitude becomes enough high. However, quantitative analyses

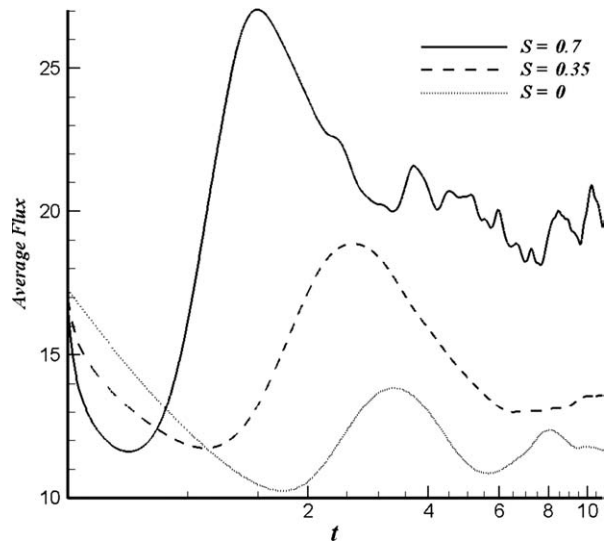

Figure 10. Variation of the average flux of carbon dioxide at the boundary for different dispersion strength values at $\alpha = 0.2$ and $Ra = 500$.

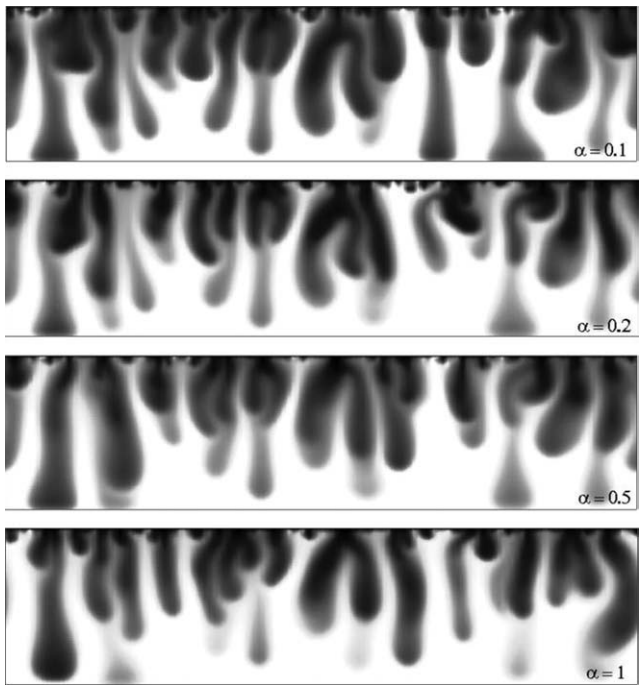

Figure 11. Concentration contours of dissolved carbon dioxide for different medium dispersivity ratios at $S = 0.7$, $t = 11$, and $Ra = 500$.

by measuring the flux, mixing length, and average concentration of the dissolved CO_2 indicate slight differences for different scenarios. In fact, one may conclude that medium dispersivity ratios may only affect the fingering pattern, while having a negligible impact on the mixing process. These results are somewhat different with a horizontal system with an initial injection velocity and viscosity difference, where the medium dispersivity ratio played a significant role.[14] However, for higher Rayleigh numbers, the velocity magnitude can reach larger values, may vary and needs further investigation. Consequently, one may conclude for such a system, which is initially at a stationary condition and with the range of parameters studied here, the dissolution of CO_2 may be only affected by dispersion strength. Medium dispersivity was found to have an impact only on the fingering pattern.

Figure 12 depicts the variation of the swept area by the dissolved CO_2 with time. In this analysis, a concentration threshold of 0.05 is assumed. The curves clearly present the three zones discussed in Figure 3, where the transition from diffusion to convection and highly nonlinear interaction can be simply realized. The curves closely overshadow each other, representing the slight effect of the medium dispersivity ratios on the convective mixing during the CO_2 sequestration process.

Figure 12 also indicates that the system with anisotropy can saturate the medium with dissolved CO_2 slightly faster. The medium is almost swept by dissolved CO_2 around the dimensionless time of 10. To scale back the system to real time, we may simply convert the times. For instance, for a slice of an aquifer (40 m $\times$ 160 m) in which the permeability, porosity, viscosity, and density differences are 67 mD,

0.22, 0.82 mPa s, and 6 kg/m^3, respectively, the dimensionless time of 10 represents 580 years.

Further investigation can be conducted by measuring the average flux at the boundary for a highly dispersive system and different medium dispersivity ratios. Figure 13 indicates the variation of the average flux for different medium dispersivity ratios. It is clear that the flux is slightly affected by medium dispersivity ratios; however, the flux is larger when medium dispersivity is decreased. This may be attributed to the slightly larger velocity values for the smaller medium dispersivity ratio. The sharp decrease in the flux later in the process may be attributed to the medium saturation by the dissolved CO_2 and also by the fingers touching the bottom of aquifer. In particular, one may notice that the onset time of convection remains almost unchanged for all scenarios. In general, it can be concluded that the effect of medium dispersivity ratios on the CO_2 sequestration process is small.

Summary and Conclusions

Thorough examinations were conducted to determine how anisotropic dispersion may affect the dissolution of carbon dioxide into brine during a sequestration process. Dispersion influences the physics of the flow system during the convective mixing process and makes the hydrodynamics of the flow more complex. We considered a simple rectilinear geometry with aspect ratios of four, where the dissolution of carbon dioxide was affected by dispersion. Dispersion has been presented by a tensor, which was velocity dependent in all directions. Generally, we highlight the impact of this velocity dependent dispersion tensor on the development of instability at a diffusive unstable boundary layer.

The results revealed that the dispersion strength highly affects the fingering patterns. It was shown that dispersion can enhance the mixing and reduce the onset of convection. In fact, higher dispersion means faster dissolution of carbon dioxide into brine. From a quantitative analysis, one may find that the sequestration process, including dispersion, may be categorized in three different zones. First, the mass transfer is dominated by diffusion; then, a transition occurs to the second zone, where convection starts and dissolution of carbon dioxide becomes dominated by convective mixing. Finally, dissolution of carbon dioxide gets faster as the rate of changes of some properties, like mixing length, flux at the boundary or average concentration of dissolved carbon dioxide, becomes faster. In fact, the third zone is dominated by highly nonlinear interactions of fingers.

The analysis also showed that the medium dispersivity ratios slightly affect the mixing. The fingering trend was only changed at longer times, where the velocities were larger. The quantitative analysis for such flow systems revealed that the medium is saturated with dissolved carbon dioxide around the same time for different anisotropies. It can be generally concluded that dispersion can play a significant role during a carbon dioxide sequestration process. In particular, the strength of dispersion in aquifers will be of great importance.

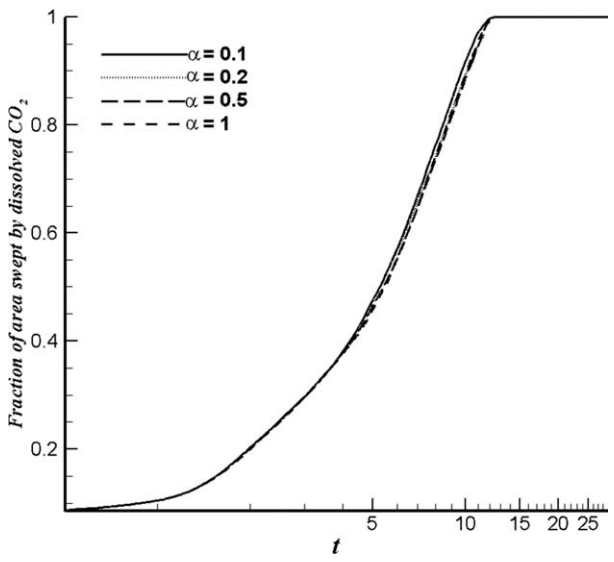

Figure 12. Variation of the swept area by dissolved CO_2 for different medium dispersivity ratios over time at $S = 0.7$ and $Ra = 500$.

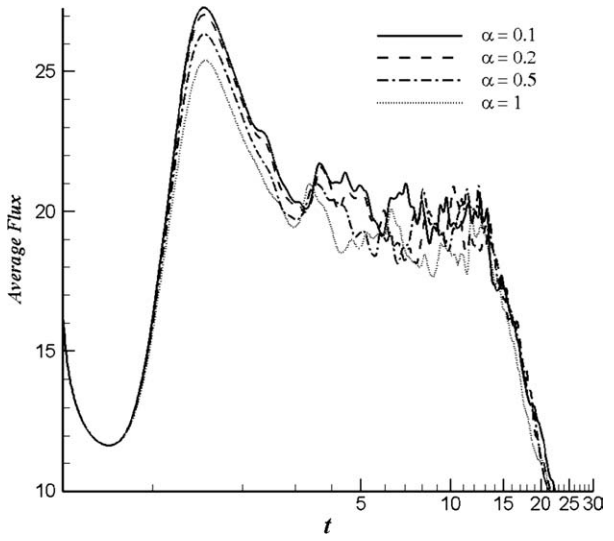

Figure 13. Variation of the average flux at the boundary for different medium dispersivity ratios vs. time at $S = 0.7$ and $Ra = 500$.

Literature Cited

1. Flette M, Gurton R, Taggart I. The function of gas-water relative permeability hysteresis in the sequestration of carbon dioxide in saline formations. SPE 88485, 2004.
2. Ennis-King J, Preston I, Paterson L. Onset of convection in anisotropic porous media subject to a rapid change in boundary conditions. *Phys Fluids*. 2005;17:084107.
3. Hassanzadeh H, Pooladi-Darvish M, Keith DW. Scaling behavior of convective mixing, with application to geological storage of CO_2. *AIChE J*. 2007;53:1121–1131.
4. Riaz A, Hesse M, Tchelepi A, Orr FM. Onset of convection in a gravitationally unstable diffusive boundary layer in porous media. *J Fluid Mech*. 2006;548:87–111.
5. Ennis-King J, Paterson L. Coupling of geochemical reactions and convective mixing in the long term geological storage of carbon dioxide. *Int J Greenhouse Gas Control*. 2007;1:86–93.
6. Gunter WD, Wiwcharb B, Perkins EH. Aquifer disposal of CO_2-rich greenhouse gases: extension of the time scale of experiment for CO_2

sequestering-reactions by geochemical modeling. *Mineral Petrol*. 1997;59:121–140.
7. Gunter WD, Perkins EH, McCann TJ. Aquifer disposal of CO_2-rich gases: reaction design for added capacity. *Energy Cons Manage*. 1993;34:941–948.
8. Tan CT, Homsy GM. Stability of miscible displacement in porous media-rectlinear flow. *Phys Fluids*. 1986;29:3549.
9. Yortsos YC, Zeybek M. Dispersion driven instability in miscible displacement in porous media. *Phys Fluids*. 1988;31:3511.
10. Zimmerman WB, Homsy GM. Nonlinear viscous fingering in miscible displacement with anisotropic dispersion. *Phys Fluids A*. 1991;3: 1859.
11. Zimmerman WB, Homsy GM. Viscous fingering in miscible displacement: unification of effects of viscosity contrast, anisotropic dispersion, and velocity dependence of dispersion on nonlinear finger propagation. *Phys Fluids A*. 1992;4:1901.
12. Petitjeans P, Chen CY, Meiburg A, Maxworthy T. Miscible quarter five-spot displacements in a Hele-Shaw cell and the role of flow-induced dispersion. *Phys Fluids*. 1999;11:1705.
13. Riaz A, Pankiewitz E, Meiburg E. Linear stability of radial displacements in porous media: influence of velocity-induced dispersion and concentration-dependent diffusion. *Phys Fluids*. 2004; 16:3592.
14. Ghesamt K, Azaiez J. Viscous fingering instability in porous media: effect of anisotropic velocity dependent dispersion tensor. *Transp Porous Med*. 2008;73:297–318.
15. Gelhar LW, Welty C, Rehfeldt K. A critical review of data on field-scale dispersion in aquifers. *Water Res*. 1992;28:1955.
16. Koch DL, Brady JF. Dispersion in fixed beds. *J Fluid Mech*. 1985;154:399–427.
17. Sahimi M, Hughes BD, Scriven LE, Davis HT. Dispersion in flow through porous media. I. One-phase flow. *Chem Eng Sci*. 1986;41: 2103–2122.
18. Bear J, Bachmat Y. *Introduction to Modelling of Transport Phenomena in Porous Media*. The Netherlands: Kluwer Academic Publishers, 1990.
19. Hidalgo J, Carrera J. Effect of dispersion on the onset of convection during CO_2 sequestration. *J Fluid Mech*. 2009;640:443–454.
20. Pau GSH, Bell JE, Pruess K, Almgren AS, Lijewski MJ, Zhang K. High-resolution simulation and characterization of density-driven flow in CO_2 storage in saline aquifers. *Adv Water Res*. 2010;33: 443–445.
21. Tchelepi HA, Orr FM. The interaction of viscous fingering, permeability heterogeneity and gravity segregation in three dimensions. *SPE Reservoir Engineering* 1994;9:266–271.

Manuscript received Dec. 24, 2009, and revision received Apr. 1, 2010.